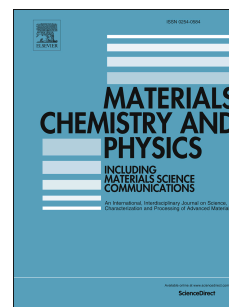# Accepted Manuscript

Monoclinic bismuth vanadate band gap determination by photoelectrochemical spectroscopy

Mikalai V. Malashchonak, Eugene A. Streltsov, Dzianis A. Kuliomin, Anatoly I. Kulak, Alexander V. Mazanik

Please cite this article as: M.V. Malashchonak, E.A. Streltsov, D.A. Kuliomin, A.I. Kulak, A.V. Mazanik, Monoclinic bismuth vanadate band gap determination by photoelectrochemical spectroscopy, *Materials Chemistry and Physics* (2017), doi: 10.1016/j.matchemphys.2017.08.053.

Monoclinic bismuth vanadate band gap determination by photoelectrochemical spectroscopy

Mikalai V. Malashchonak[a], Eugene A. Streltsov[a], Dzianis A. Kuliomin[b],

Anatoly I. Kulak[b], Alexander V. Mazanik[a,*]

[a]Belarusian State University, Nezalezhnastsi Av. 4, 220030 Minsk, Belarus

[b]Institute of General and Inorganic Chemistry, National Academy of Sciences of Belarus,

Surganov St. 9/1, 220072 Minsk, Belarus

E-mail: mazanikalexander@gmail.com; Fax: +375-17-2095445; Tel: +375-29-2769624.

Highlights

- Optical band gap of monoclinic $BiVO_4$ was determined by photocurrent spectroscopy;

- Indirect optical transitions are characterized by the energy E_{gi}=2.44 eV;

- Direct optical transitions are characterized by the energy E_{gd}=2.63 eV;

Abstract

The optical band gap (E_g) of the monoclinic bismuth vanadate $BiVO_4$ (scheelite) was determined by photoelectrochemical (photocurrent) spectroscopy. The relevance of this study is related to an existing ambiguity in E_g determination, which is due to possible distinction in preparation technique of this compound (and, hence, difference in grain size, crystallinity, film thickness, etc.), as well as realization of additional optical absorption mechanisms unrelated to excitation of electrons from the valence band to the conduction band. Using analysis of the Incident Photon-to-current Conversion Efficiency (IPCE), which minimizes a contribution of impurity-related and other kinds of absorption, it was demonstrated that $BiVO_4$ scheelite is primarily indirect

band gap semiconductor, where indirect optical transitions are characterized by the energy gap E_{gi}=2.44 eV, whereas for direct optical transitions energy gap is E_{gd}=2.63 eV.

Keywords:

Bismuth vanadate; Band gap; Photocurrent spectroscopy.

1. Introduction

In the last decade the interest in optical properties of monoclinic bismuth vanadate has significantly increased due to its high activity in photocatalytic [1-7] and photoelectrochemical (PEC) [6-10] processes. An important advantage of monoclinic $BiVO_4$ over classical photocatalytic oxides (TiO_2, ZnO, WO_3) is its smaller band gap (E_g) which allows photoinduced processes under irradiation not only by UV but also by the visible part of the spectrum. E_g values of monoclinic $BiVO_4$ estimated from the long-wavelength edge of the diffuse reflectance spectra are in the range 2.33–2.50 eV [1,3,8,11]. The band gap for direct optical transitions (E_{gd}) calculated from the diffuse reflectance spectra using the Kubelka-Munk function by some authors [5,6,12-14] was 2.45–2.46 eV, while higher values were reported by other authors: 2.48 eV [15], 2.52–2.56 eV [16], 2.60 eV [17], 2.68 eV [18]. The information concerning the values of indirect optical transitions band gap (E_{gi}) is more limited; in particular, according to G. Li et al. [19], E_{gi} value is 2.20 eV; O.F. Lopez et al. determined E_{gi} to be in the range from 2.35 to 2.42 eV [20], while from the results of P. Madhusudan et al. [4] E_{gi} values are 2.34 and 2.13 eV for polycrystalline and porous $BiVO_4$, respectively. Despite the fact that the vast majority of workers determined E_g values for the direct optical transitions, recently it has been proved conclusively that monoclinic $BiVO_4$ is indirect-gap semiconductor with E_{gi} value equal to 2.52 eV [18].

The ambiguity in determining the band gap values and optical transitions type in monoclinic $BiVO_4$ is not only due to the difference in the preparation technique (accordingly,

differences in crystallite size, the ordering degree, film thickness, etc.), but also due to the presence of additional mechanisms of optical absorption without excitation of electrons from the valence band to the conduction band of semiconductor [21]. In particular, this kind of parasitic absorption in hydrogenated $BiVO_4$ was observed at a wavelength $\lambda > 530$ nm (photon energy $h\nu < 2.34$ eV) without contribution to photogeneration processes responsible for PEC activity of $BiVO_4$ photoanode [22].

Considering the foregoing discussion, in the present study the photocurrent spectroscopy has been used to determine the band gap of monoclinic $BiVO_4$. Photocurrent flows as a result of the generation of electron-hole pairs due to the interband absorption of photons with energy $h\nu \geq E_g$ with the subsequent involvement of the photogenerated charge carriers in a photoelectrochemical reactions. The advantage of this method of E_g determination in comparison with classical optical methods is the minimum impact of other absorption mechanisms besides the fundamental interband transitions in the photocurrent spectrum.

At the same time, the Incident Photon-to-current Conversion Efficiency (IPCE, Y) evaluated from photocurrent spectrum can be considered as $Y(\lambda)=Y_1(\lambda)\cdot Y_2(\lambda)$, where $Y_1(\lambda)$ is the fraction of incident photons resulted in electron-hole pair generation (proportional to the absorption coefficient near the absorption edge), and $Y_2(\lambda)$ is the fraction of the photogenerated charge carriers participating in photoelectrochemical reactions (determined by recombination losses, i.e. by relation between film thickness, diffusion length, surface recombination rate and depth of photocharges generation) [23]. It is obvious that spectral dependence of Y_2 can distort the obtained E_g value. Recently it has been shown that the photocurrent generated on $BiVO_4$ is not limited by surface reaction kinetics, but by surface recombination [24]. Therefore, to verify the correctness of E_g determination from IPCE spectra, it is necessary to compare results of E_g calculation obtained under different recombination impact. Such variation can be achieved by changing the film permeability for electrolyte, as well as photocharge generation depth. So, the

films with different porosity have been studied and different geometries of their illumination have been used.

2. Experimental

BiVO$_4$ film electrodes were prepared by spin-coating (3000 rpm) of BiVO$_4$ colloidal solution on optically transparent substrate with a layer of electrically conductive fluorine-doped tin oxide (FTO). The colloidal solution was prepared by mixing of 0.75 mol/L Bi(NO$_3$)$_3$ and 0.075 mol/L of NH$_4$VO$_3$ aqueous solutions taken in a volume ratio of 1 : 10 followed by centrifugation, 5 times washing with distilled water and ultrasonical dispersing (44 kHz, 10 minutes) with the addition of 30% aqueous ammonia solution (1:100 per volume) as a colloid stabilizer. To increase the porosity of BiVO$_4$ films, a 10% solution of polyvinyl alcohol (PVA) was added to BiVO$_4$ colloid in a ratio of 1:1 by volume. According to the adsorption analysis (Brunauer–Emmett–Teller method [25], N$_2$ adsorption at 77 K, ASAP 2020 surface area and porosity analyser, Micromeritics, USA), the addition of a pore-forming PVA increases the specific surface of the film from 3.2 to 5.8 m^2/g and a specific pore volume from 0.006 to 0.011 cm^3/g. Hereafter, the BiVO$_4$ films synthesized without and with PVA will be referred as "dense" and "porous", respectively.

The heat treatment of prepared films in air at 450 ^{o}C for 2 hours resulted in the formation of monoclinic crystal structure of BiVO$_4$ according to XRD and Raman spectroscopy (see below). From SEM results, the deposited BiVO$_4$ films were found to have a thickness of several hundred nanometers. These films are composed of rounded or elongated particles with a relatively small area of contact with each other (Fig. S1a). The addition of PVA to the suspension results in the subsequent partial fusion of BiVO$_4$ particles (Fig. S1b). Despite such fusion of particles, the specific surface and pore volume increases by 1.8 – 2 times due to the formation of an additional porous during the thermal oxidation of PVA additive.

4

XRD patterns were taken in the Bragg-Brentano geometry with a Bruker D8 Advance diffractometer using Cu Kα radiation. The average size (r) of crystallites was evaluated by the Scherrer formula from the half-width of the XRD peak corrected for the instrumental broadening: $r = 0.9\lambda_{K\alpha}/B_{2\Theta}\cos\Theta$, where $\lambda_{K\alpha}$ is 0.15406 nm for copper anode, $B_{2\Theta}$ is the full width at half-maximum of diffraction peak (2Θ scale, in radians).

Raman spectra were recorded at room temperature in the range of Raman shifts from 70 to 2400 cm^{-1} using a Nanofinder HE confocal spectrometer (LOTIS TII, Belarus – Japan) equipped with a solid-state laser (λ=532 nm), 600 lines/mm grating (providing a spectral resolution better than 2.5 cm^{-1}) and a thermostated CCD camera.

Photocurrent spectra were obtained using a setup equipped with a MDR-23U high-intensity grating monochromator (spectral resolution 1 nm), a halogen lamp (250 W power, color temperature of 3350 K) and a light chopper (frequency of 0.3 s^{-1}). The potential of the semiconductor electrode was controlled by a P-8 potentiostat (Elins, Russia) equipped with a three-electrode quartz cell with a saturated silver chloride reference electrode (+0.201 V vs. SHE) and a platinum auxiliary electrode. 0.1 mol/L Na_2SO_3 aqueous solution was used as electrolyte, which is optically transparent in the $BiVO_4$ absorption area and can effectively scavenge the photogenerated holes. High electrical conductivity of the used solution (1.44 $\Omega^{-1}m^{-1}$ at 25 °C [26]) ensured insignificance of iR drop. IPCE was calculated from the photocurrent and the light intensity at the monochromator output measured by an OPT101P silicon photodiode (TI Burr-Brown, USA). Band-gap energies are presented as the mean value for the set of three individual samples. Standard deviation was calculated with statistical software of OriginPro 7.0 (OriginLab Corporation, USA).

Transmission and diffuse reflectance spectra were measured using an Agilent 8453 (Agilent Technologies, USA) and a Specord M40 (Carl Zeiss Jena, Germany) spectrometers, respectively, with spectral resolution about 1 nm.

3. Results and Discussion

The identification of the crystal structure of the obtained $BiVO_4$ samples was carried out by comparison of their XRD patterns (Fig. 1a,c) and Raman spectra (Fig. 1b,d) with the literature [5,10,27-29].
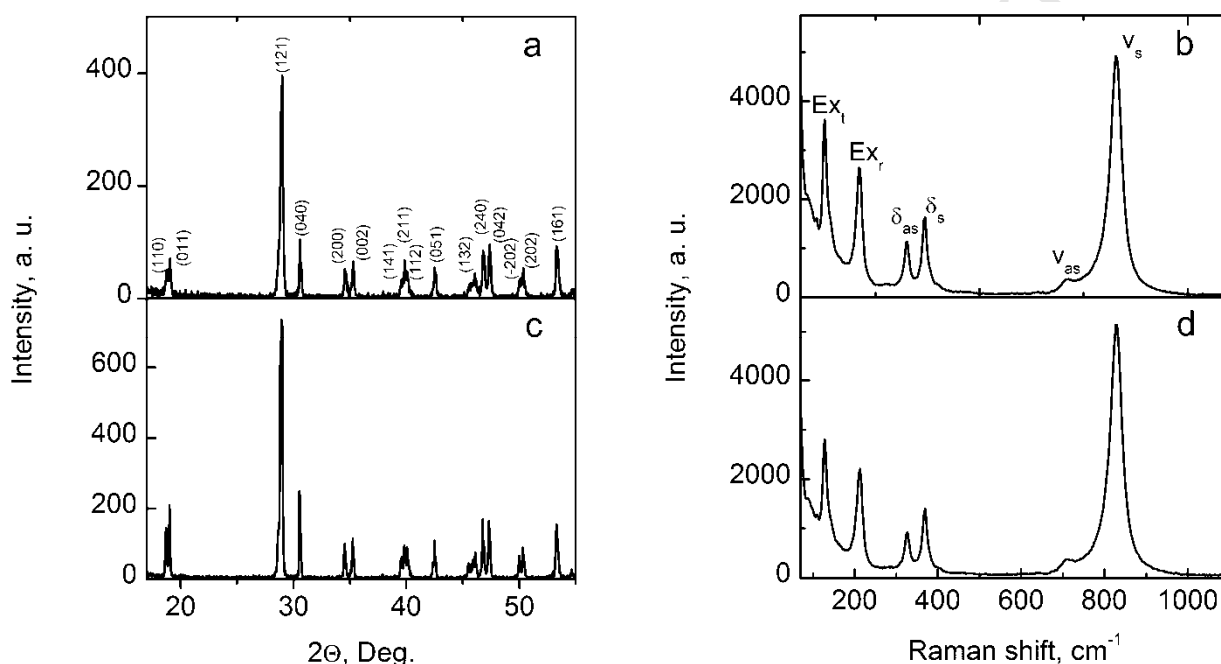

Fig 1. XRD patterns (a, c) and Raman spectra (b, d) of "dense" (a, b) and "porous" (c, d) $BiVO_4$ films heat treated at 450 ^{o}C.

XRD patterns of the grown films demonstrate only reflexes inherent to monoclinic scheelite-type $BiVO_4$. From broadening of XRD reflexes using the Scherrer equation, a grain size in the $BiVO_4$ films can be estimated as appr. 70 nm for "dense" and appr. 85 nm for "porous" films that exceeds significantly the Bohr radius of exciton, which is calculated to be equal to ≈9 nm (taking into account that $m_e=0.9m_0$ and $m_h=0.7m_0$ [30], ε=68 [31]. Thus, one can neglect electron quantum confinement effect on the IPCE spectra of the studied $BiVO_4$ films.

In the Raman spectra, the bands at 127 and 213 cm^{-1} are associated with translational Ex_t and rotational Ex_r phonon vibration modes, at 325 and 367 cm^{-1} – with asymmetrical δ_{as} and symmetrical δ_s bending vibrations in VO_4^{3-} tetrahedra, at 707 and 827 cm^{-1} – with asymmetrical

6

ν_{as} and symmetrical ν_s stretching vibrations in VO_4^{3-} tetrahedra in $BiVO_4$ monoclinic scheelite-type phase [5,10,27-29]. $BiVO_4$ films prepared using a pore-forming additive PVA have the similar spectral band positions ~~with a slight difference in ν_s band position which is shifted to the high-frequency region by 3 cm^{-1} and has a half-width increased from 32 to 35 cm^{-1}.~~

Thus, XRD and Raman spectroscopy results demonstrate that $BiVO_4$ films used in this study have the scheelite-type monoclinic crystal structure regardless of their porosity. It should be noted that bismuth vanadate with such structure has a higher photoelectrochemical and photocatalytic activity in the visible range with respect to other crystal modifications in particular tetragonal one [8,12,32-34].

$BiVO_4$ electrodes generate anodic photocurrent in Na_2SO_3 solution. Their illumination through an optically transparent FTO substrate (Fig. 2a) or through an electrolyte layer (Fig. 2b) results in slightly different photocurrent spectra. Primarily, this difference is caused by non-equilibrium carrier recombination losses on the way from the photogeneration area. No matter which side of the film was illuminated, the distance to be overcome by photoholes to reach the semiconductor/electrolyte interface is equal to a "feature size" of the films [35] (a few tens of nanometers in the present case, Fig. S1). On the contrary, the distance to be overcome by the photoelectrons depends on what side is illuminated. When electrode is illuminated through the FTO substrate, the photogeneration process is mainly concentrated near this substrate, and electrons overcome a minimal distance to achieve the FTO layer providing higher IPCE values in contrast to irradiation from the solution side (see. Fig. 2). It should be noted that $BiVO_4$ electrode prepared using a pore-forming additive PVA (curves 2 and 4) has a higher photocurrent in comparison with the "dense" film electrode (curves 1 and 3), which is naturally explained by more developed electrode/electrolyte interface in the case of the "porous" film.
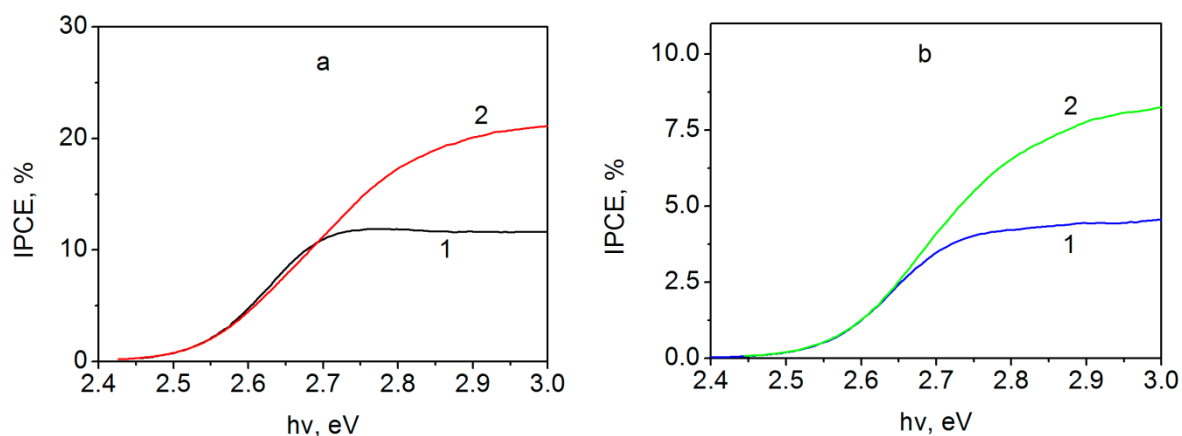
Fig. 2. IPCE spectra of the "dense" (curves 1 and 3) and "porous" (curves 2 and 4) $BiVO_4$ electrodes in 0.1 mol/L Na_2SO_3 aqueous solution. Electrode potential is 400 mV vs. Ag/AgCl; electrode system was irradiated from the FTO substrate side (a) and from the solution side (b).

Taking into account the proportional dependence of IPCE (Y) on the optical absorption coefficient (α) [23], the values E_{gd} and E_{gi} can be determined by extrapolation of the linear part of $(Yh\nu)^2 - h\nu$ dependencies for direct and $(Yh\nu)^{1/2} - h\nu$ dependencies for indirect optical transitions on the energy axis. As it is seen from Figs. 3, 4, the linearization of the IPCE spectra is possible for $(Yh\nu)^2 - h\nu$, and for $(Yh\nu)^{1/2} - h\nu$ dependencies. It indicates that both direct and indirect optical transitions occur for $BiVO_4$ scheelite monoclinic modification.
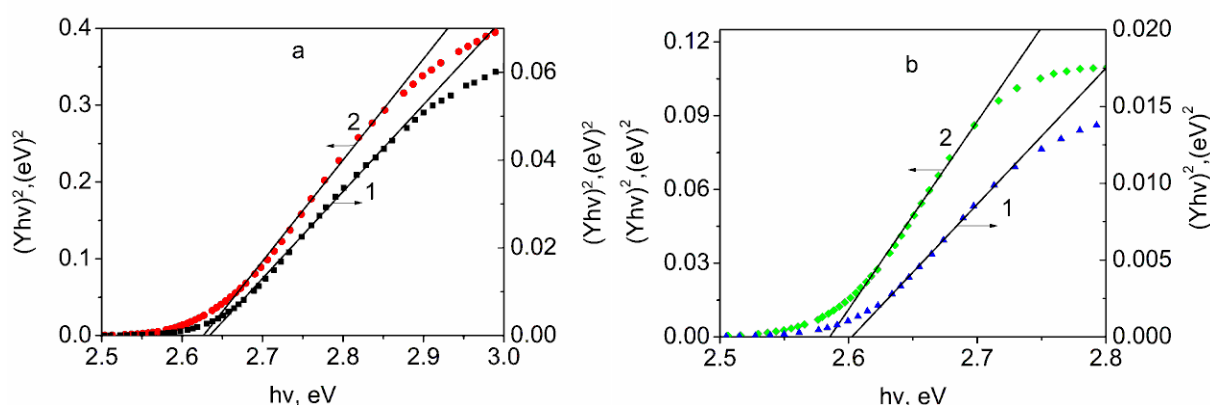

Fig. 3. Determination of the band gap for direct optical transitions from the spectral dependencies of IPCE for "dense" (1) and "porous" (2) $BiVO_4$ films; irradiation of the electrode from the FTO substrate side (a) and from the solution side (b).

8

Fig. 4. Determination of the band gap for indirect optical transitions from the spectral dependencies of IPCE for "dense" (1) and "porous" (2) $BiVO_4$ films; irradiation of the electrode from the FTO substrate side (a) and from the solution side (b).
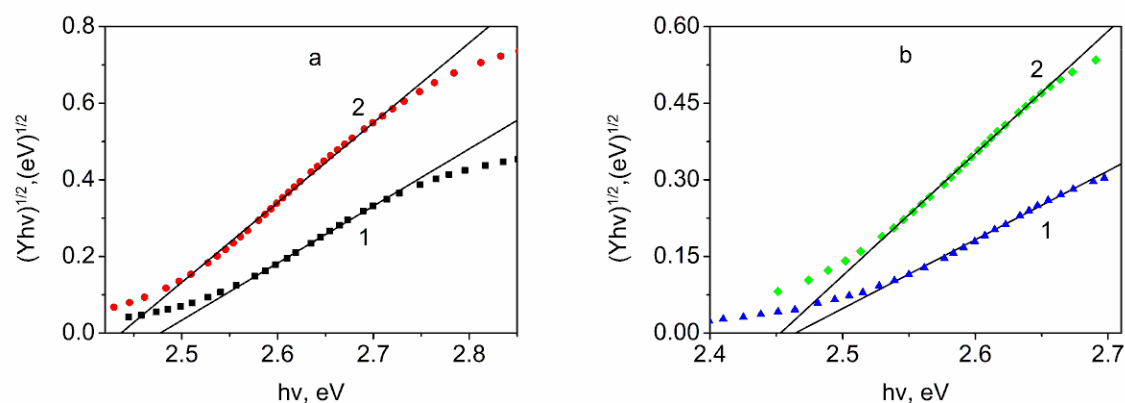
E_{gd} and E_{gi} values determined from the spectra are almost identical (within error) for the "dense" and "porous" $BiVO_4$ films and weakly depend on the illuminated side (substrate or solution) (Tab. 1). E_{gi} values determined from $(Yh\nu)^{1/2}$–$h\nu$ dependencies (Fig. 4) obtained for irradiating of the electrode from the solution side are 2.45–2.46 eV for both "dense" and "porous" $BiVO_4$ films. If the irradiation was carried out from the conductive substrate, E_{gi} value for "dense" films is slightly increased.

As it can be seen, E_g values determined from transmission (Fig. S2) and diffuse reflectance (Fig. S3) spectra are significantly smaller as compared to those extracted from photocurrent spectra, which can be related to absorption mechanisms not attributed to interband electron transitions.

Obtained data reveals that the band gap of indirect optical transitions for "dense" and "porous" $BiVO_4$ films is 0.14 eV lower than the band gap of direct optical transitions when the illumination of the electrode was carried out from the solution side. The difference between E_{gd} and E_{gi} is 0.15 eV for the "dense" and 0.19 eV for the "porous" $BiVO_4$ films when the illumination was carried out from the FTO substrate side.

9

Table 1
The parameters of IPCE spectral dependencies linearization for BiVO$_4$ electrodes in a solution containing 0.1 mol/L Na$_2$SO$_3$.

Film type	Illumination side	Optical transition type	Linearization range, eV	Band gap value, eV	Determination coefficient R^2
Dense	solution	direct	2.62–2.73	2.60±0.03	0.999
Porous	solution	direct	2.60–2.70	2.58±0.03	0.996
Dense	substrate	direct	2.65–2.86	2.63±0.03	0.998
Porous	substrate	direct	2.65–2.85	2.63±0.03	0.996
Dense	solution	indirect	2.52–2.68	2.46±0.03	0.997
Porous	solution	indirect	2.52–2.65	2.45±0.01	0.999
Dense	substrate	indirect	2.58–2.73	2.48±0.03	0.998
Porous	substrate	indirect	2.55–2.75	2.44±0.02	0.996

It should be noted that the E_{gd} and E_{gi} values for BiVO$_4$ scheelite monoclinic modification recently obtained using the complex spectral methods were 2.68 and 2.52 eV [18], the difference between E_{gd} and E_{gi} was 0.16 eV. These values are in good agreement with our E_{gd} and E_{gi} values determined in a significantly different way – by analyzing the photocurrent spectra. Small (0.05 eV) excess of E_{gd} value given in [18] above the value obtained in our study, when illumination of the electrode was carried out from the FTO substrate side, presumably, can be attributed to the quantum confinement effect, which may appear in BiVO$_4$ films used in the work [18]. We can explain the 0.04 eV difference between the E_{gi} value for "dense" BiVO$_4$ films and the data for E_{gi} given in [18] in a similar way. Slightly lower E_{gd} and E_{gi} values obtained for the irradiation of the electrode from the solution side can be attributed to the light scattering effect when it passes through the film to the photogenerated carriers separation area which is located near the contact with the FTO. Similar effect was observed ~~in~~ for ZnO films covered by SILAR grown CdS nanoparticles [36].

As it was mentioned above, charge carrier recombination can affect E_g values determined from IPCE spectra. Since the illumination of "porous" films from the conductive FTO substrate

side provides the maximal IPCE values (minimal recombination impact), the corresponding values $E_{gi} = 2.44$ eV and $E_{gd} = 2.63$ eV could be probably considered as the most reliable ones.

4. Conclusions

$BiVO_4$ film electrodes with different porosity have been prepared by spin-coating method. Their single-phase scheelite-type monoclinic crystal structure has been revealed by XRS and Raman spectroscopy methods, and the optical band gap has been found from the anodic photocurrent spectra. The photoelectrochemically determined most reliable value of the indirect optical transition band gap E_{gi} for $BiVO_4$ scheelite monoclinic phase is considered to be 2.44 eV (obtained for "porous" films under irradiation from the FTO substrate side). Accordingly, E_{gd} value for direct optical transitions is 2.63 eV. Obtained E_{gd} and E_{gi} values, in our opinion, are the most useful in the interpretation of spectral efficiency dependencies of photocatalytic and photoelectrochemical processes, since these values are obtained not from the optical diffuse reflection spectra, but from the photocurrent spectra, which give the efficiency of photoelectrochemical reactions under illumination. Although the band gap determination in this case is based on the linear dependence of IPCE on the optical absorption coefficient of the semiconductor, the impact of the impurity absorption and other types of absorption not associated with the excitation of electrons from the valence band into conduction band of semiconductor is minimized in the spectral dependence of the quantum efficiency.

Acknowledgments

11

References

[1] J. Yu, A. Kudo, Effects of structural variation on the photocatalytic performance of hydrothermally synthesized $BiVO_4$, Adv. Funct. Mater. 16 (2006) 2163–2169, http://dx.doi.org/10.1002/adfm.200500799.

[2] N.C. Castillo, L. Ding, A. Heel, T. Graule, C. Pulgarin, On the photocatalytic degradation of phenol and dichloroacetate by $BiVO_4$: The need of a sacrificial electron acceptor, J. Photochem. Photobiol. A 216 (2010) 221–227, http://dx.doi.org/10.1016/j.jphotochem.2010.08.021.

[3] S.S. Dunkle, R.J. Helmich, K.S. Suslick, $BiVO_4$ as a visible-light photocatalyst prepared by ultrasonic spray pyrolysis, J. Phys. Chem. C 113 (2009) 11980–11983, http://dx.doi.org/10.1021/jp903757x.

[4] P. Madhusudan, M.V. Kumar, T. Ishigaki, K. Toda, K. Uematsu, M. Sato, Hydrothermal synthesis of meso/macroporous $BiVO_4$ hierarchical particles and their photocatalytic degradation properties under visible light irradiation, Environ. Sci. Pollut. Res. 20 (2013) 6638–6645, http://dx.doi.org/10.1007/s11356-013-1694-x.

[5] S.M. Thalluri, C.M. Suarez, M. Hussain, S. Hernandez, A. Virga, G. Saracco, N. Russo, Evaluation of the parameters affecting the visible-light-induced photocatalytic activity of monoclinic $BiVO_4$ for water oxidation, Ind. Eng. Chem. Res. 52 (2013) 17414–17418, http://dx.doi.org/10.1021/ie402930x.

[6] K.P.S. Parmar, H.J. Kang, A. Bist, P. Dua, J.S. Jang, J.S. Lee, Photocatalytic and photoelectrochemical water oxidation over metal-doped monoclinic $BiVO_4$ photoanodes, ChemSusChem. 5 (2012) 1926–1934, http://dx.doi.org/10.1002/cssc.201200254.

[7] H. K. Timmaji, W. Chanmanee, N. R. de Tacconi and K. Rajeshwar, Solution combustion synthesis of BiVO$_4$ nanoparticles: effect of combustion precursors on the photocatalytic activity, J. Adv. Oxid. Technol. 14 (2011) 93–105.

[8] A. Iwase, A. Kudo, Photoelectrochemical water splitting using visible-light-responsive BiVO$_4$ fine particles prepared in an aqueous acetic acid solution, J. Mater. Chem. 20 (2010) 7536–7542, http://dx.doi.org/10.1039/c0jm00961j.

[9] T.W. Kim, K.-S. Choi, Nanoporous BiVO$_4$ photoanodes with dual-layer oxygen evolution catalysts for solar water splitting, Science 343 (2014) 990–994, http://dx.doi.org/10.1126/science.1246913.

[10] Y. Liang, T. Tsubota, L.P.A. Mooij, R. van de Krol, Highly improved quantum efficiencies for thin film BiVO$_4$ photoanodes, J. Phys. Chem. C 115 (2011) 17594–17598, http://dx.doi.org/10.1021/jp203004v.

[11] R. Venkatesan, S. Velumani, A. Kassiba, Mechanochemical synthesis of nanostructured BiVO$_4$ and investigations of related features, Mater. Chem. Phys. 135 (2012) 842–848, http://dx.doi.org/10.1016/j.matchemphys.2012.05.068.

[12] G. Li, Y. Bai, W.F. Zhang, Difference in valence band top of BiVO$_4$ with different crystal structure, Mater. Chem. Phys. 136 (2012) 930–934, http://dx.doi.org/10.1016/j.matchemphys.2012.08.023.

[13] Y. Sun, Y. Xie, C. Wu, S. Zhang, S. Jiang, Aqueous synthesis of mesostructured BiVO$_4$ quantum tubes with excellent dual response to visible light and temperature, Nano Res. 3 (2010) 620–631, http://dx.doi.org/10.1007/s12274-010-0022-8.

[14] L. Zhou, W. Wang, S. Liu, L. Zhang, H. Xu, W. Zhu, A sonochemical route to visible-light-driven high-activity BiVO$_4$ photocatalyst, J. Mol. Catal. A: Chem. 252 (2006) 120–124, http://dx.doi.org/10.1016/j.molcata.2006.01.052.

[15] D.J. Payne, M. Robinson, R.G. Egdell, A. Walsh, J. McNulty, K.E. Smith, L.F.J. Piper, The nature of electron lone pairs in $BiVO_4$, Appl. Phys. Lett. 98 (2011) 212110, http://dx.doi.org/10.1063/1.3593012.

[16] S. Stoughton, M. Showak, Q. Mao, P. Koirala, D.A. Hillsberry, S. Sallis, L.F. Kourkoutis, K. Nguyen, L.F.J. Piper, D.A. Tenne, N.J. Podraza, D.A. Muller, C. Adamo, D.G. Schlom, Adsorption-controlled growth of $BiVO_4$ by molecular-beam epitaxy, APL Mater. 1 (2013) 042112, http://dx.doi.org/10.1063/1.4824041.

[17] H. Gong, N. Freudenberg, M. Nie, R. van de Krol, K. Ellmer, $BiVO_4$ photoanodes for water splitting with high injection efficiency, deposited by reactive magnetron co-sputtering, AIP Adv. 6 (2016) 045108, http://dx.doi.org/10.1063/1.4947121.

[18] J.K. Cooper, S. Gul, F.M. Toma, L. Chen, Y.-S. Liu, J. Guo, J.W. Ager, J. Yano, I.D. Sharp, Indirect bandgap and optical properties of monoclinic bismuth vanadate, J. Phys. Chem. C 119 (2015) 2969–2974, http://dx.doi.org/10.1021/jp512169w.

[19] G. Li, D. Zhang, J.C. Yu, Ordered mesoporous $BiVO_4$ through nanocasting: a superior visible light-driven photocatalyst, Chem. Mater. 20 (2008) 3983–3992, http://dx.doi.org/10.1021/cm800236z.

[20] O.F. Lopes, K.T. Carvalho, A.E. Nogueira, W. Avansi, C. Ribeiro, Controlled synthesis of $BiVO_4$ photocatalysts: Evidence of the role of heterojunctions in their catalytic performance driven by visible-light, Appl. Catal. B: Environ. 188 (2016) 87–97, http://doi.org/10.1016/j.apcatb.2016.01.065.

[21] P. Y. Yu, M. Cardona, Fundamentals of Semiconductors; Springer: Berlin–Heidelberg–New York, 2005.

[22] G. Wang, Y. Ling, X. Lu, F. Qian, Y. Tong, J.Z. Zhang, V. Lordi, C.R. Leao, Y. Li, Computational and photoelectrochemical study of hydrogenated bismuth vanadate, J. Phys. Chem. C 117 (2013) 10957–10964, http://dx.doi.org/10.1021/jp401972h.

[23] Y.V. Pleskov, Solar Energy Conversion, Springer-Verlag, Heidelberg, 1990.

[24] C. Zachäus, F.F. Abdi, L.M. Peter, R. van de Krol, Photocurrent of $BiVO_4$ is limited by surface recombination, not surface catalysis, Chem. Sci. 8 (2017) 3712–3719, http://doi.org/10.1039/C7SC00363C.

[25] S. Gregg, K. Sing, Adsorption Surface Area and Porosity, Academic Press, London, 1982.

[26] W. M. Haynes, CRC Handbook of Chemistry and Physics, 94th Edition, CRC Press, Taylor & Francis, 2013.

[27] R.L. Frost, D.A. Henry, M.L. Weier, W. Martens, Raman spectroscopy of three polymorphs of $BiVO_4$: clinobisvanite, dreyerite and pucherite, with comparisons to $(VO_4)_3$-bearing minerals: namibite, pottsite and schumacherite, J. Raman Spectrosc. 37 (2006) 722–732, http://dx.doi.org/10.1002/jrs.1499.

[28] M.S. Jang, H.L. Park, J.N. Kim, J.H. Ro, Y.H. Park, Raman spectrum in monoclinic $BiVO_4$, Jpn. J. Appl. Phys. 24 (1985) 506–507.

[29] F.D. Hardcastle, I.E. Wachs, H. Eckert, D.A. Jefferson, Vanadium(V) environments in bismuth vanadates: A structural investigation using Raman spectroscopy and solid state [51]V NMR, J. Solid State Chem. 90 (1991) 194–210, http://dx.doi.org/10.1016/0022-4596%2891%2990135-5.

[30] Z. Zhao, Z. Li, Z. Zou, Electronic structure and optical properties of monoclinic clinobisvanite $BiVO_4$, Phys. Chem. Chem. Phys., 2011, 13, 4746 – 4753, http://dx.doi.org/10.1039/C0CP01871F.

[31] M. Zalfani, M. Mahdouani, R. Bourguiga, B.L. Su, Experimental and theoretical study of optical properties and quantum size phenomena in the $BiVO_4/TiO_2$ nanostructures, Superlattices Microstruct. 83 (2015) 730–744, http://dx.doi.org/10.1016/j.spmi.2015.04.020.

15

[32] Y. Liu, B. Huang, Y. Dai, X. Zhang, X. Qin, M. Jiang, M.H. Whangbo, Selective ethanol formation from photocatalytic reduction of carbon dioxide in water with $BiVO_4$ photocatalyst, Catal. Commun. 11 (2009) 210–213, http://dx.doi.org/10.1016/j.catcom.2009.10.010.

[33] S. Tokunaga, H. Kato, A. Kudo, Selective preparation of monoclinic and tetragonal $BiVO_4$ with scheelite structure and their photocatalytic properties, Chem. Mater. 13 (2001) 4624–4628, http://dx.doi.org/10.1021/cm0103390.

[34] A. Kudo, K. Omori, H. Kato, A novel aqueous process for preparation of crystal form-controlled and highly crystalline $BiVO_4$ powder from layered vanadates at room temperature and its photocatalytic and photophysical properties, J. Am. Chem. Soc. 121 (1999) 11459 –11467, http://dx.doi.org/10.1021/ja992541y.

[35] J.A. Seabold, K. Zhu, N.R. Neale, Efficient solar photoelectrolysis by nanoporous $Mo:BiVO_4$ through controlled electron transport, Phys.Chem.Chem.Phys. 16 (2014) 1121–1131, http://dx.doi.org/10.1039/c3cp54356k.

[36] M.V. Malashchonak, E.A. Streltsov, A.V. Mazanik, A.I. Kulak, S.K. Poznyak, O.L. Stroyuk, S.Ya. Kuchmiy, P.I. Gaiduk, Band-gap and sub-band-gap photoelectrochemical processes at nanocrystalline CdS grown on ZnO by successive ionic layer adsorption and reaction method, Thin Solid Films 589 (2015) 145–152, http://dx.doi.org/10.1016/j.tsf.2015.04.057.
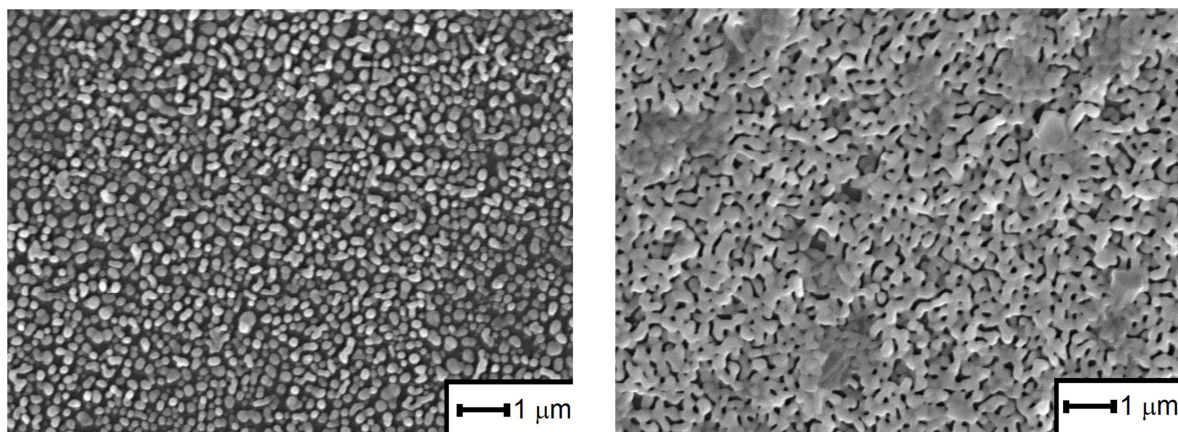
Supplementary Information

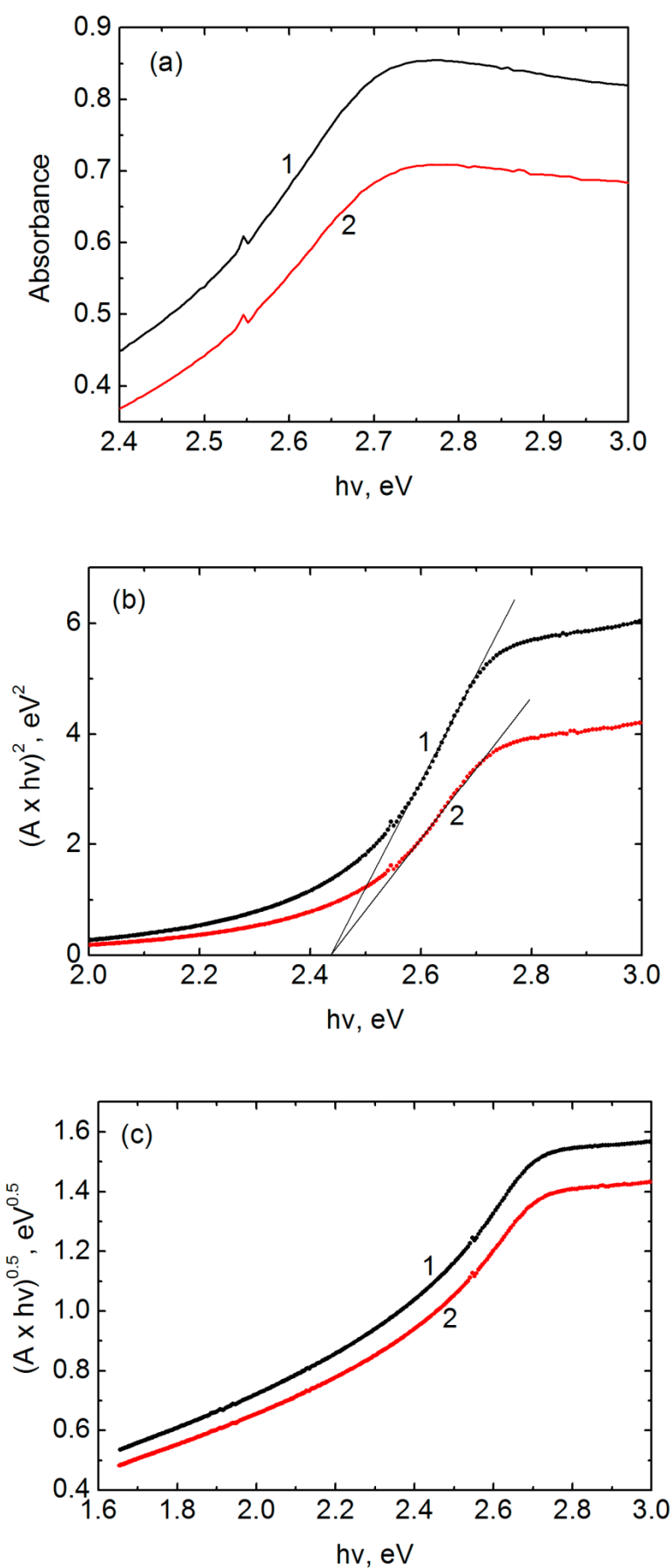**Fig. S1.** SEM images of "dense" (on the left) and "porous" (on the right) BiVO$_4$ films.

Fig. S2. Transmission spectra of the "dense" (curves 1) and "porous" (curves 2) BiVO$_4$ films (a) and their linearization in the Tauc coordinates for direct (b) and indirect (c) optical transitions.
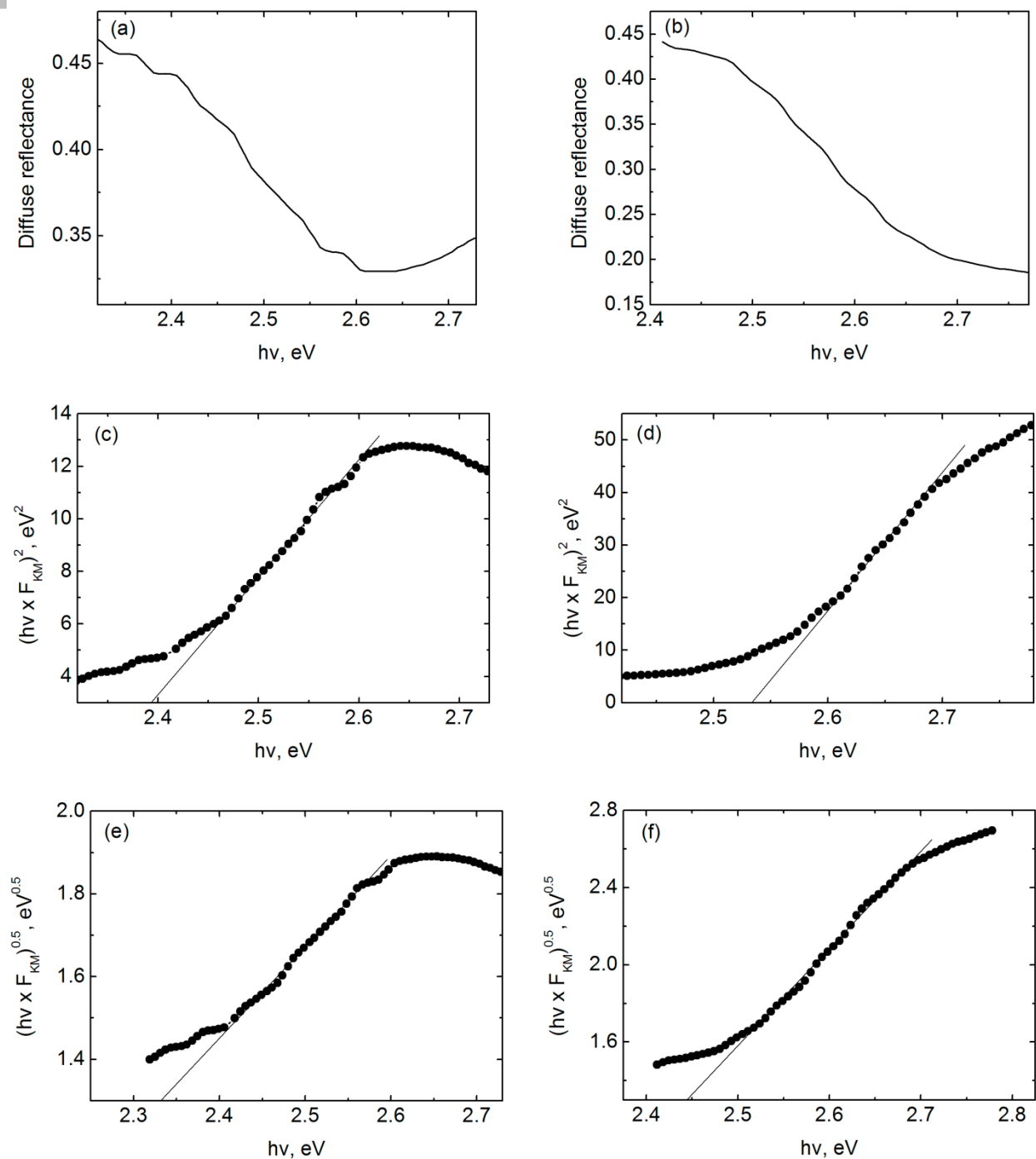
Fig. S3. Diffuse reflectance spectra of the "dense" (a) and "porous" (b) BiVO$_4$ films and their linearization in the Tauc coordinates for direct (c, d) and indirect (e, f) optical transitions with the Kubelka – Munk function.